Longitudinal double-spin asymmetry for inclusive jet and dijet production in polarized proton collisions at $\sqrt{s} = 510$ GeV

M. S. Abdallah[5], B. E. Aboona[55], J. Adam[6], L. Adamczyk[2], J. R. Adams[39], J. K. Adkins[30], G. Agakishiev[28], I. Aggarwal[41], M. M. Aggarwal[41], Z. Ahammed[60], I. Alekseev[3,35], D. M. Anderson[55], A. Aparin[28], E. C. Aschenauer[6], M. U. Ashraf[11], F. G. Atetalla[29], A. Attri[41], G. S. Averichev[28], V. Bairathi[53], W. Baker[10], J. G. Ball Cap[20], K. Barish[10], A. Behera[52], R. Bellwied[20], P. Bhagat[27], A. Bhasin[27], J. Bielcik[14], J. Bielcikova[38], I. G. Bordyuzhin[3], J. D. Brandenburg[6], A. V. Brandin[35], I. Bunzarov[28], X. Z. Cai[50], H. Caines[63], M. Calderón de la Barca Sánchez[8], D. Cebra[8], I. Chakaberia[31,6], P. Chaloupka[14], B. K. Chan[9], F-H. Chang[37], Z. Chang[6], N. Chankova-Bunzarova[28], A. Chatterjee[11], S. Chattopadhyay[60], D. Chen[10], J. Chen[49], J. H. Chen[18], X. Chen[48], Z. Chen[49], J. Cheng[57], M. Chevalier[10], S. Choudhury[18], W. Christie[6], X. Chu[6], H. J. Crawford[7], M. Csanád[16], M. Daugherity[1], T. G. Dedovich[28], I. M. Deppner[19], A. A. Derevschikov[43], A. Dhamija[41], L. Di Carlo[62], L. Didenko[6], P. Dixit[22], X. Dong[31], J. L. Drachenberg[1], E. Duckworth[29], J. C. Dunlop[6], N. Elsey[62], J. Engelage[7], G. Eppley[45], S. Esumi[58], O. Evdokimov[12], A. Ewigleben[32], O. Eyser[6], R. Fatemi[30], F. M. Fawzi[5], S. Fazio[6], P. Federic[38], J. Fedorisin[28], C. J. Feng[37], Y. Feng[44], P. Filip[28], E. Finch[51], Y. Fisyak[6], A. Francisco[63], C. Fu[11], L. Fulek[2], C. A. Gagliardi[55], T. Galatyuk[15], F. Geurts[45], N. Ghimire[54], A. Gibson[59], K. Gopal[23], X. Gou[49], D. Grosnick[59], A. Gupta[27], W. Guryn[6], A. I. Hamad[29], A. Hamed[5], Y. Han[45], S. Harabasz[15], M. D. Harasty[8], J. W. Harris[63], H. Harrison[30], S. He[11], W. He[18], X. H. He[26], Y. He[49], S. Heppelmann[8], S. Heppelmann[42], N. Herrmann[19], E. Hoffman[20], L. Holub[14], Y. Hu[18], H. Huang[37], H. Z. Huang[9], S. L. Huang[52], T. Huang[37], X. Huang[57], Y. Huang[57], T. J. Humanic[39], G. Igo[9,*], D. Isenhower[1], W. W. Jacobs[25], C. Jena[23], A. Jentsch[6], Y. Ji[31], J. Jia[6,52], K. Jiang[48], X. Ju[48], E. G. Judd[7], S. Kabana[53], M. L. Kabir[10], S. Kagamaster[32], D. Kalinkin[25,6], K. Kang[57], D. Kapukchyan[10], K. Kauder[6], H. W. Ke[6], D. Keane[29], A. Kechechyan[28], M. Kelsey[62], Y. V. Khyzhniak[35], D. P. Kikoła[61], C. Kim[10], B. Kimelman[8], D. Kincses[16], I. Kisel[17], A. Kiselev[6], A. G. Knospe[32], H. S. Ko[31], L. Kochenda[35], L. K. Kosarzewski[14], L. Kramarik[14], P. Kravtsov[35], L. Kumar[41], S. Kumar[26], R. Kunnawalkam Elayavalli[63], J. H. Kwasizur[25], R. Lacey[52], S. Lan[11], J. M. Landgraf[6], J. Lauret[6], A. Lebedev[6], R. Lednicky[28,38], J. H. Lee[6], Y. H. Leung[31], N. Lewis[6], C. Li[49], C. Li[48], W. Li[45], X. Li[48], Y. Li[57], X. Liang[10], Y. Liang[29], R. Licenik[38], T. Lin[49], Y. Lin[11], M. A. Lisa[39], F. Liu[11], H. Liu[25], H. Liu[11], P. Liu[52], T. Liu[63], X. Liu[39], Y. Liu[55], Z. Liu[48], T. Ljubicic[6], W. J. Llope[62], R. S. Longacre[6], E. Loyd[10], N. S. Lukow[54], X. F. Luo[11], L. Ma[18], R. Ma[6], Y. G. Ma[18], N. Magdy[12], D. Mallick[36], S. Margetis[29], C. Markert[56], H. S. Matis[31], J. A. Mazer[46], N. G. Minaev[43], S. Mioduszewski[55], B. Mohanty[36], M. M. Mondal[52], I. Mooney[62], D. A. Morozov[43], A. Mukherjee[16], M. Nagy[16], J. D. Nam[54], Md. Nasim[22], K. Nayak[11], D. Neff[9], J. M. Nelson[7], D. B. Nemes[63], M. Nie[49], G. Nigmatkulov[35], T. Niida[58], R. Nishitani[58], L. V. Nogach[43], T. Nonaka[58], A. S. Nunes[6], G. Odyniec[31], A. Ogawa[6], S. Oh[31], V. A. Okorokov[35], B. S. Page[6], R. Pak[6], J. Pan[55], A. Pandav[36], A. K. Pandey[58], Y. Panebratsev[28], P. Parfenov[35], B. Pawlik[40], D. Pawlowska[61], C. Perkins[7], L. Pinsky[20], R. L. Pintér[16], J. Pluta[61], B. R. Pokhrel[54], G. Ponimatkin[38], J. Porter[31], M. Posik[54], V. Prozorova[14], N. K. Pruthi[41], M. Przybycien[2], J. Putschke[62], H. Qiu[26], A. Quintero[54], C. Racz[10], S. K. Radhakrishnan[29], N. Raha[62], R. L. Ray[56], R. Reed[32], H. G. Ritter[31], M. Robotkova[38], O. V. Rogachevskiy[28], J. L. Romero[8], D. Roy[46], L. Ruan[6], J. Rusnak[38], A. K. Sahoo[22], N. R. Sahoo[49], H. Sako[58], S. Salur[46], J. Sandweiss[63,*], S. Sato[58], W. B. Schmidke[6], N. Schmitz[33], B. R. Schweid[52], F. Seck[15], J. Seger[13], M. Sergeeva[9], R. Seto[10], P. Seyboth[33], N. Shah[24], E. Shahaliev[28], P. V. Shanmuganathan[6], M. Shao[48], T. Shao[18], A. I. Sheikh[29], D. Y. Shen[18], S. S. Shi[11], Y. Shi[49], Q. Y. Shou[18], E. P. Sichtermann[31], R. Sikora[2], M. Simko[38], J. Singh[41], S. Singha[26], M. J. Skoby[44], N. Smirnov[63], Y. Söhngen[19], W. Solyst[25], P. Sorensen[6], H. M. Spinka[4,*], B. Srivastava[44], T. D. S. Stanislaus[59], M. Stefaniak[61], D. J. Stewart[63], M. Strikhanov[35], B. Stringfellow[44], A. A. P. Suaide[47], M. Sumbera[38], B. Summa[42], X. M. Sun[11], X. Sun[12], Y. Sun[48], Y. Sun[21], B. Surrow[54], D. N. Svirida[3], Z. W. Sweger[8], P. Szymanski[61], A. H. Tang[6], Z. Tang[48], A. Taranenko[35], T. Tarnowsky[34], J. H. Thomas[31], A. R. Timmins[20], D. Tlusty[13], T. Todoroki[58], M. Tokarev[28], C. A. Tomkiel[32], S. Trentalange[9], R. E. Tribble[55], P. Tribedy[6], S. K. Tripathy[16], T. Truhlar[14], B. A. Trzeciak[14], O. D. Tsai[9], Z. Tu[6], T. Ullrich[6], D. G. Underwood[4,59], I. Upsal[45], G. Van Buren[6], J. Vanek[38], A. N. Vasiliev[43], I. Vassiliev[17], V. Verkest[62], F. Videbæk[6], S. Vokal[28], S. A. Voloshin[62], F. Wang[44], G. Wang[9], J. S. Wang[21], P. Wang[48], X. Wang[49], Y. Wang[11], Y. Wang[57], Z. Wang[49], J. C. Webb[6], P. C. Weidenkaff[19], L. Wen[9], G. D. Westfall[34], H. Wieman[31], S. W. Wissink[25], J. Wu[11], J. Wu[26], Y. Wu[10], B. Xi[50], Z. G. Xiao[57], G. Xie[31], W. Xie[44], H. Xu[21], N. Xu[31], Q. H. Xu[49], Y. Xu[49], Z. Xu[6], Z. Xu[9], G. Yan[49], C. Yang[49], Q. Yang[49],

S. Yang[45], Y. Yang[37], Z. Ye[45], Z. Ye[12], L. Yi[49], K. Yip[6], Y. Yu[49], H. Zbroszczyk[61], W. Zha[48], C. Zhang[52], D. Zhang[11], J. Zhang[49], S. Zhang[12], S. Zhang[18], X. P. Zhang[57], Y. Zhang[26], Y. Zhang[48], Y. Zhang[11], Z. J. Zhang[37], Z. Zhang[6], Z. Zhang[12], J. Zhao[44], C. Zhou[18], Y. Zhou[11], X. Zhu[57], M. Zurek[4], M. Zyzak[17]

(STAR Collaboration)

[1]Abilene Christian University, Abilene, Texas 79699
[2]AGH University of Science and Technology, FPACS, Cracow 30-059, Poland
[3]Alikhanov Institute for Theoretical and Experimental Physics NRC "Kurchatov Institute", Moscow 117218, Russia
[4]Argonne National Laboratory, Argonne, Illinois 60439
[5]American University of Cairo, New Cairo 11835, New Cairo, Egypt
[6]Brookhaven National Laboratory, Upton, New York 11973
[7]University of California, Berkeley, California 94720
[8]University of California, Davis, California 95616
[9]University of California, Los Angeles, California 90095
[10]University of California, Riverside, California 92521
[11]Central China Normal University, Wuhan, Hubei 430079
[12]University of Illinois at Chicago, Chicago, Illinois 60607
[13]Creighton University, Omaha, Nebraska 68178
[14]Czech Technical University in Prague, FNSPE, Prague 115 19, Czech Republic
[15]Technische Universität Darmstadt, Darmstadt 64289, Germany
[16]ELTE Eötvös Loránd University, Budapest, Hungary H-1117
[17]Frankfurt Institute for Advanced Studies FIAS, Frankfurt 60438, Germany
[18]Fudan University, Shanghai, 200433
[19]University of Heidelberg, Heidelberg 69120, Germany
[20]University of Houston, Houston, Texas 77204
[21]Huzhou University, Huzhou, Zhejiang 313000
[22]Indian Institute of Science Education and Research (IISER), Berhampur 760010 , India
[23]Indian Institute of Science Education and Research (IISER) Tirupati, Tirupati 517507, India
[24]Indian Institute Technology, Patna, Bihar 801106, India
[25]Indiana University, Bloomington, Indiana 47408
[26]Institute of Modern Physics, Chinese Academy of Sciences, Lanzhou, Gansu 730000
[27]University of Jammu, Jammu 180001, India
[28]Joint Institute for Nuclear Research, Dubna 141 980, Russia
[29]Kent State University, Kent, Ohio 44242
[30]University of Kentucky, Lexington, Kentucky 40506-0055
[31]Lawrence Berkeley National Laboratory, Berkeley, California 94720
[32]Lehigh University, Bethlehem, Pennsylvania 18015
[33]Max-Planck-Institut für Physik, Munich 80805, Germany
[34]Michigan State University, East Lansing, Michigan 48824
[35]National Research Nuclear University MEPhI, Moscow 115409, Russia
[36]National Institute of Science Education and Research, HBNI, Jatni 752050, India
[37]National Cheng Kung University, Tainan 70101
[38]Nuclear Physics Institute of the CAS, Rez 250 68, Czech Republic
[39]Ohio State University, Columbus, Ohio 43210
[40]Institute of Nuclear Physics PAN, Cracow 31-342, Poland
[41]Panjab University, Chandigarh 160014, India
[42]Pennsylvania State University, University Park, Pennsylvania 16802
[43]NRC "Kurchatov Institute", Institute of High Energy Physics, Protvino 142281, Russia
[44]Purdue University, West Lafayette, Indiana 47907
[45]Rice University, Houston, Texas 77251
[46]Rutgers University, Piscataway, New Jersey 08854
[47]Universidade de São Paulo, São Paulo, Brazil 05314-970
[48]University of Science and Technology of China, Hefei, Anhui 230026
[49]Shandong University, Qingdao, Shandong 266237
[50]Shanghai Institute of Applied Physics, Chinese Academy of Sciences, Shanghai 201800
[51]Southern Connecticut State University, New Haven, Connecticut 06515
[52]State University of New York, Stony Brook, New York 11794
[53]Instituto de Alta Investigación, Universidad de Tarapacá, Arica 1000000, Chile
[54]Temple University, Philadelphia, Pennsylvania 19122
[55]Texas A&M University, College Station, Texas 77843
[56]University of Texas, Austin, Texas 78712
[57]Tsinghua University, Beijing 100084
[58]University of Tsukuba, Tsukuba, Ibaraki 305-8571, Japan
[59]Valparaiso University, Valparaiso, Indiana 46383

[60]Variable Energy Cyclotron Centre, Kolkata 700064, India

[61]Warsaw University of Technology, Warsaw 00-661, Poland

[62]Wayne State University, Detroit, Michigan 48201

[63]Yale University, New Haven, Connecticut 06520 and

[*]Deceased

We report measurements of the longitudinal double-spin asymmetry, A_{LL}, for inclusive jet and dijet production in polarized proton-proton collisions at midrapidity and center-of-mass energy $\sqrt{s}$ = 510 GeV, using the high luminosity data sample collected by the STAR experiment in 2013. These measurements complement and improve the precision of previous STAR measurements at the same center-of-mass energy that probe the polarized gluon distribution function at partonic momentum fraction $0.015 \lesssim x \lesssim 0.25$. The dijet asymmetries are separated into four jet-pair topologies, which provide further constraints on the x dependence of the polarized gluon distribution function. These measurements are in agreement with previous STAR measurements and with predictions from current next-to-leading order global analyses. They provide more precise data at low dijet invariant mass that will better constraint the shape of the polarized gluon distribution function of the proton.

Over the last 20 years, the STAR experiment at the Relativistic Heavy Ion Collider (RHIC) has used high-energy polarized proton collisions with center-of-mass energies up to 510 GeV to gain deeper insight into the spin structure and dynamics of the proton. One of the major goals of the RHIC spin program is to perform high precision measurements of the polarized gluon distribution function of the proton, $\Delta g(x, Q^2)$, where x is the partonic momentum fraction and Q^2 is the momentum transfer. These measurements are motivated by previous analyses from other experiments, starting from the results of polarized Deep Inelastic Scattering (DIS) experiments in the late 1980's, that showed the proton spin could not originate only from the quarks, thereby initiating experimental searches for the gluon contribution to the proton spin (see [1] and references therein).

The kinematic coverage at STAR provides access to gluons through the quark-gluon and gluon-gluon scatterings which dominate particle production at low and medium values of transverse momentum at RHIC. Previous STAR longitudinal double-spin asymmetry (A_{LL}) measurements of inclusive jets with pseudorapidity $|\eta| < 1$ [2] and dijets with $|\eta| < 0.8$ [3], from data collected during the year 2009 with center-of-mass energy of 200 GeV, strongly suggest a non-zero gluon polarization for $x > 0.05$. The latest global analysis fits, DSSV14 [4] and NNPDFpol1.1 [5], which include the 2009 STAR inclusive jet measurements [2], extract a positive contribution to the proton spin coming from gluon spin; however, the uncertainty remains large for $x < 0.05$.

It has been suggested that dijet production should be an effective observable to extract the x dependence of the gluon polarization, since dijets provide better constraints on the underlying kinematics, $e.g.$, compared to inclusive observables [6]. At leading order, the dijet invariant mass is proportional to the square root of the product of the partonic momentum fractions, $M_{inv} = \sqrt{sx_1x_2}$, and the pseudorapidity sum of the two jets is proportional to the logarithmic ratio of the x values, $\eta_3 + \eta_4 \propto \log(x_1/x_2)$ [7]. Measurements at both $\sqrt{s} = 200$ GeV and 510 GeV provide broad kinematic coverage in x. The wide acceptance of the STAR detector permits reconstruction of dijet events with different topological configurations, $i.e.$, different pseudorapidity combinations that probe symmetric ($x_1 = x_2$) and asymmetric ($x_1 < x_2$ or $x_1 > x_2$) partonic collisions.

STAR has also measured A_{LL} for dijet production with one or both jets in $0.8 < \eta < 1.8$, using the data collected during 2009 at $\sqrt{s} = 200$ GeV [8]. A reweighting study of the DSSV14 fit was performed using the 2009 STAR dijet data [3, 8]. The results of this reweighted fit had a clear impact on our understanding of the gluon polarization in the region of $x \gtrsim 0.2$ [9].

The first STAR inclusive jet and dijet A_{LL} measurements in longitudinally polarized proton collisions at $\sqrt{s}$ = 510 GeV and midrapidity $|\eta| < 0.9$ were performed using data recorded in 2012 [10], presenting good agreement with previous results in the overlapping x region. In 2015, STAR concluded the longitudinally polarized proton program with another $\sqrt{s} = 200$ GeV data set. The 2015 inclusive jet and dijet results at midrapidity [11] are consistent and have better precision than the previous measurements [2, 3], providing further evidence of a positive gluon polarization for $x > 0.05$. Both the 2012 and 2015 results will provide new constraints on the gluon polarization at $0.015 \lesssim x \lesssim 0.25$ and $0.05 \lesssim x \lesssim 0.5$, respectively, when they are included in future global analyses. Other measurements to constrain the gluon polarization include inclusive pion production by PHENIX at midrapidity [12, 13], and by STAR at $2.65 < \eta < 3.9$ [14], which provides sensitivity down to $x \sim 0.001$.

In this paper, we report measurements of A_{LL} for inclusive jet and dijet production at $\sqrt{s} = 510$ GeV using the data recorded by STAR during 2013 in the region $|\eta| < 0.9$. The luminosity was approximately 250 pb^{-1}, which is almost three times higher than the previ-

ous year. The longitudinal double-spin asymmetry A_{LL} calculations follow the same procedure as [2, 3, 10, 11]:

$$A_{LL} = \frac{\Sigma_{runs} P_Y P_B (N^{++} - r N^{+-})}{\Sigma_{runs} P_Y^2 P_B^2 (N^{++} + r N^{+-})}, \qquad (1)$$

where P_B and P_Y are the measured polarizations of the beams (denoted Blue and Yellow), N^{++} and N^{+-} are the jet or dijet yields for equal and opposite proton beam helicity configurations, and r is the relative luminosity, which is the ratio of the luminosities for different helicity configurations of the colliding beams. The beam polarizations and the relative luminosities were reasonably constant during individual experimental runs, which were each about 30 minutes in length throughout a 7-8 hour RHIC fill. The relative luminosity had a multimodal distribution that varied between 0.87 and 1.12 (average 1.002), depending on beam conditions $e.g.$, polarization pattern and beam intensity. The polarizations of the beams were measured for each RHIC fill by a proton-carbon based Coulomb-Nuclear Interference polarimeter [15], calibrated by using a polarized hydrogen gas-jet target [16]. The average polarizations were $P_B = 56\%$ and $P_Y = 54\%$, with a 6.4% relative uncertainty on the product of the beam polarizations [17].

The main tracking device at STAR is a Time Projection Chamber (TPC) in a 0.5 T solenoidal magnetic field. The TPC acceptance is $|\eta| \lesssim 1.3$ and 2π in the azimuthal angle (ϕ) [18]. The Barrel Electromagnetic Calorimeter (BEMC) [19] and the Endcap Electromagnetic Calorimeter (EEMC) [20] were used to trigger on jets and measure their electromagnetic constituents. The BEMC covers $|\eta| \leq 1.0$ and the EEMC $1.1 < \eta < 2.0$, both with full azimuthal coverage. The helicity-dependent relative luminosity was calculated using the Vertex Position Detectors (VPD) [21] and Zero Degree Calorimeters (ZDC) [22].

Events were recorded if they satisfied a jet patch (JP) trigger condition [10, 23], which was defined by requiring that the BEMC or EEMC detected a transverse energy that exceeded one of the three thresholds equivalent to 6.8 GeV for JP0, 9.0 GeV for JP1 and 14.4 GeV for JP2, over an area of approximately $\Delta\eta \times \Delta\phi = 1 \times 1$. In addition to the JP triggers, two new triggers, "JP0dijet" and "JP1dijet", were introduced for this measurement. These new triggers required that one JP met the JP0 or JP1 energy threshold, and that a second JP met a threshold of 2.8 GeV, with the two JPs required to be nonadjacent in ϕ. All JP2 events were collected while JP1dijet and JP0dijet were prescaled (one dijet per three and twelve triggered events, respectively). The JP1 and JP0 triggers were highly prescaled (around one in forty and two hundred triggered events, respectively) in order to reserve data acquisition bandwidth for the dijet triggers.

The anti-k_T algorithm [24] and FastJet [25] package were used to reconstruct jets. The jet resolution parameter for this analysis was $R = 0.5$, in contrast to the studies

at $\sqrt{s} = 200$ GeV that used $R = 0.6$ [2, 3, 11]. This parameter was lowered for the 510 GeV measurements [10] to reduce sensitivity to underlying event effects. The individual tracks and towers had to meet certain conditions, similar to the quality assurance requirements as in [10]. The tracks from the TPC that were used in the jet finding algorithm satisfied a transverse momentum $p_T > 0.2$ GeV/c, had at least 12 hit points in the TPC with more than 51% of the possible hits along the reconstructed track segment, were associated to a collision vertex located within $\pm$ 90 cm of the nominal interaction point, and followed a p_T-dependent distance of closest approach (DCA) to the vertex. The DCA requirements were: less than 2 cm for $p_T < 0.5$ GeV/c, less than 1 cm for $p_T > 1.5$ GeV/c, and linearly interpolated between these two points. The BEMC and EEMC towers were required to have a transverse energy of $E_T > 0.2$ GeV. If a track pointed to the tower, the track p_T (multiplied by c) was subtracted from the tower E_T to avoid double counting of particles which were fully reconstructed by both the TPC and calorimeters. The fraction of jet energy detected in the calorimeters (R_{EM}) was required to be less than 0.95.

For inclusive jets, only the JP0, JP1, and JP2 triggered events were considered. Software cuts in p_T were applied above the trigger thresholds to JP0 = 7.0 GeV/c, JP1 = 9.6 GeV/c and JP2 = 15.3 GeV/c, to reduce reconstruction bias near the hardware thresholds. The reconstructed jet axis was required to lie within the location of the JP that fired the trigger. Any jet containing a track with a reconstructed $p_T > 30$ GeV/c was rejected, since the TPC resolution degrades at these momenta. The summed p_T of all reconstructed tracks in the jet was required to be larger than 0.5 GeV/c to remove, for example, non-collision backgrounds. In cases where more than one jet in an event satisfied the selection criteria (approximately 5% of jet events), only the two highest p_T jets were taken.

The dijet analysis only considered the two largest p_T jets in an event. As in Ref. [10], the dijet opening-angle and pseudorapidity cuts were $\Delta\phi > 120^o$ and $|\Delta\eta| < 1.6$, to remove jets arising from hard gluon emission and to avoid having both jets fall near the detector acceptance limits. An empirical p_T-matching condition required the ratio of the leading and away-side jet transverse momenta be $p_T^{leading}/p_T^{away} < 6 - (0.08 \times p_T^{max})$, where p_T^{max} is the highest transverse momentum track in either jet, to remove fake jets [10]. An asymmetric p_T cut was applied, requiring one jet to have $p_T > 7.0$ GeV/c while the other jet had $p_T > 5.0$ GeV/c, to allow comparison with theory models [4, 5, 9]. The same software cuts in p_T as for inclusive jets were applied. At least one of the jets needed to point to the location of the JP that fired the JP0, JP1 or JP2 trigger, whereas both jets needed to match the JP0dijet or JP1dijet trigger locations.

The individual jets in a dijet were separated into three

Bin	η_3 and η_4 Regions	Physics description
A	$0.3 < |\eta_{3,4}| < 0.9$; $\eta_3 \cdot \eta_4 > 0$	Forward-Forward
B	$|\eta_{3,4}| < 0.3$; $0.3 < |\eta_{4,3}| < 0.9$	Forward-Central
C	$|\eta_{3,4}| < 0.3$	Central-Central
D	$0.3 < |\eta_{3,4}| < 0.9$; $\eta_3 \cdot \eta_4 < 0$	Forward-Backward

TABLE I. The four dijet topology bins A-D.

pseudorapidity regions: forward $0.3 < \eta < 0.9$, central $-0.3 < \eta < 0.3$, and backward $-0.9 < \eta < -0.3$. The A_{LL} measurements for dijets are presented in four topology bins A-D (see Table I), as in [10], which allows discrimination between symmetric and asymmetric collisions in terms of the partonic momentum fractions x_1 and x_2.

Inclusive jet and dijet observables were corrected for underlying event contributions using the off-axis cone method as in [10, 26]. Inclusive jet or dijet events were rejected if the ratio of the underlying event correction divided by the jet p_T or dijet M_{inv} was greater than 34% and 36%, respectively, as in [10, 11], to ensure that the jet or dijet was not shifted by more than two bin intervals of p_T or M_{inv}.

Simulation events were produced to quantify the detector response, connecting the jets at detector level to the initial partonic level. These simulated events were also used to estimate systematic uncertainties and apply a trigger bias correction. The simulations were produced using PYTHIA 6.4.28 [27] with the Perugia 2012 tune 370 [28], reducing the PARP(90) parameter to 0.213 as in [10, 11]. This parameter controls the energy dependence of the low-p_T cut for the underlying-event generation, thereby providing better agreement with STAR inclusive pion measurements [29, 30]. The full detector response was simulated with GEANT 3 [31], with the STAR configuration in 2013. The simulated events were embedded into randomly selected bunch crossings from real data to mimic real beam background, pile-up, and detector inefficiencies.

A trigger software simulator was used in the offline processing to incorporate time-dependent pedestal variations and detector efficiencies. The trigger emulator classified simulation events using the same logic as the data triggering but without prescale factors, in order to match the data to the simulation. In the case that a jet satisfied all the conditions to be classified as JP1, this event could be recorded as a JP0 trigger in the data because of the prescale; however, it would be considered as a JP1 trigger in the analysis because the emulator promotes it. Similar considerations were made for the dijet triggers.

Figure 1 shows the comparison between data and the embedded simulation of the inclusive jet counts versus p_T at the detector level. The steps in the distribution correspond to trigger thresholds. Figure 2 shows the comparison between data and the embedded simulation of dijet counts versus the invariant mass, at detector level, for the
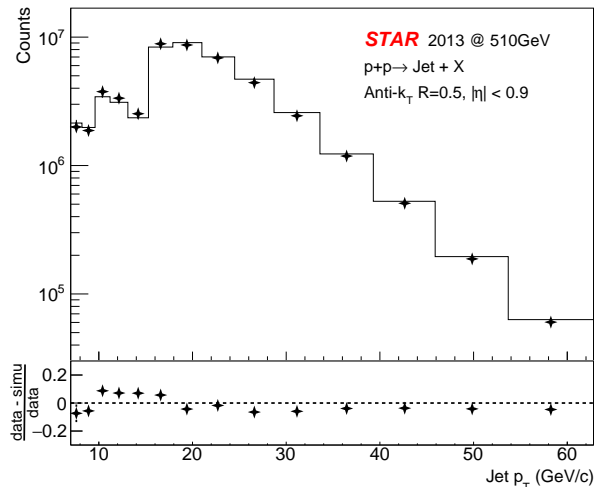

FIG. 1. Comparison between data (points) and embedded simulation (histogram) of the inclusive jet yield versus p_T at detector level. The lower panel shows the ratio of the relative differences between data and the simulation. Statistical uncertainties are smaller than most of the points.
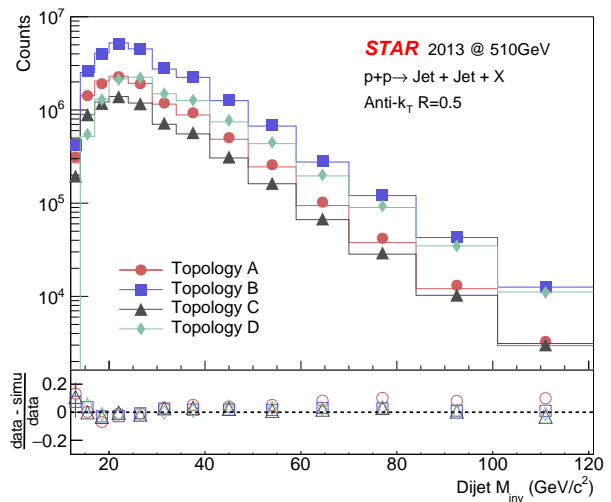

FIG. 2. Comparison between data (points) and embedded simulation (histograms) of the dijet yield versus the invariant mass, at detector level, for the different topology regions studied. The lower panel shows the ratio of the relative differences between data and the simulation. Statistical uncertainties are smaller than most of the points.

different topologies considered. The data and embedded simulation for both inclusive jet and dijet measurements agree to within 15%; these differences are small enough to be covered by the systematic uncertainties.

The reconstructed jets were unfolded bin-by-bin to the parton level in order to compare directly with the the-

oretical calculation. Detector jets were reconstructed in the simulation and matched with their partonic counterparts if the two jets were within $\sqrt{\Delta\eta^2 + \Delta\phi^2} \leq 0.5$. The closest parton jet in $\eta - \phi$ space was chosen if more than one parton jet matched a given detector jet.

The sources of systematic uncertainties considered for both the inclusive jet and dijet measurements are the same as in [10, 11]. The jet energy scale systematic uncertainties include the following: the calorimeter tower (electromagnetic response) gain and efficiency for the run conditions in 2013 contributed about 3.1% of the jet energy scale values (dominant systematic); the TPC tracking efficiency and resolution effects (hadronic response) contributed about 1.5%; the difference between data and simulation for the underlying event correction was less than 1%; and the differences between other PYTHIA tunes were about 5% in the lower jet energy scale bins, down to about 1% for the higher bins. Additionally, the statistical uncertainties of the unfolding were considered as a systematic (less than 1%).

Trigger and reconstruction bias effects were studied with the simulation to compensate for distortions due to detector finite resolution and efficiency. The efficiency of the STAR triggers varies for different partonic subprocesses (quark-quark, quark-gluon and gluon-gluon) [2, 10]. The trigger bias and the finite resolution of the detector affect the A_{LL} measurements. Corrections (within 0.00004 and 0.003) were obtained by comparing the average differences between the asymmetry for reconstructed detector jets and parton jets, by using one hundred equally probable replicas of the NNPDFpol1.1 [5] estimations. The root-mean-square of these differences, in addition to the finite statistics of the simulation, were considered as systematic uncertainties, and varied approximately from 0.0002 for lower p_T or M_{inv} bins and increased up to 0.002 for inclusive jets and 0.006 for dijets. Tables of the uncertainty values are presented in supplemental materials [32].

The underlying event correction modifies the value of the reconstructed jet energy, thus affecting the A_{LL} measurement. Another systematic uncertainty was assigned to the A_{LL} due to the underlying event correction as in [10, 11], by calculating the longitudinal double-spin asymmetry of the spin-dependent average underlying event correction for inclusive jet, $A_{LL}^{dp_T}$, and dijet, $A_{LL}^{dM_{inv}}$. These underlying event asymmetries were on average $A_{LL}^{dp_T} = 0.0006 \pm 0.0009$ for inclusive jet, $A_{LL}^{dM_{inv}} = -0.0006 \pm 0.0010$ for dijet topology A, -0.0001 $\pm$ 0.0007 for dijet topology B, -0.0015 $\pm$ 0.0013 for dijet topology C, and 0.0023 $\pm$ 0.0009 for dijet topology D. The systematic uncertainties due to this effect were below 0.0003 for inclusive jets and 0.001 for dijets, being the dominant A_{LL} systematic uncertainty at low energy scale, and dropping to less than 0.0002 at large energy scale values for both measurements. The parity-violating longitudi-

nal single-spin asymmetries A_L (for each of the two colliding beams) were consistent with zero within 2.5 standard deviations. The effect of a residual transverse beam polarization component was estimated and found to be negligible.

Figure 3 shows the 2013 inclusive jet A_{LL} (blue) as a function of the parton jet transverse momentum scaled by $2/\sqrt{s}$. The shaded blue boxes represent systematic uncertainty (width indicates the jet energy resolution), which is the quadrature sum of the trigger and reconstruction bias, the underlying event correction, plus the relative luminosity uncertainty that was estimated to be 4.7×10^{-4}. The vertical lines correspond to statistical uncertainties, including consideration of the correlation between two jets when they are found in the same event. This result is compared with previous STAR results [2, 10, 11] with all their systematic uncertainties added in quadrature, and expectations from the latest global analyses available in [4, 5]. There is good agreement among all measurements and with the global fits.
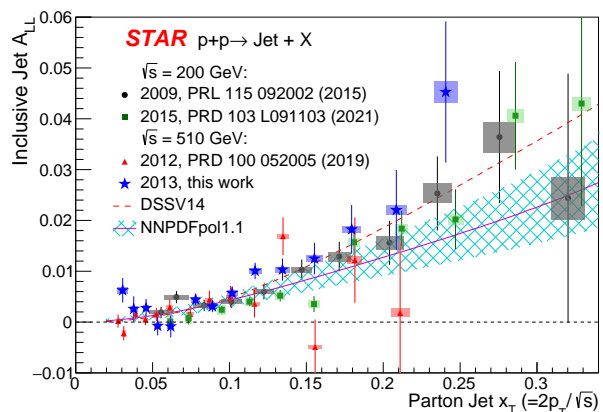

FIG. 3. Inclusive jet A_{LL} versus x_T, compared to previous STAR results at $\sqrt{s} = 200$ GeV [2, 11] and 510 GeV [10], and evaluations from DSSV14 [4] and NNPDFpol1.1 (with its uncertainty) [5] global analyses. The vertical lines are statistical uncertainties. The boxes show the size of the estimated systematic uncertainties. Scale uncertainties from polarization (not shown) are $\pm6.5\%$, $\pm6.6\%$, $\pm6.4\%$ and $\pm6.1\%$ from 2009 to 2015, respectively.

Figure 4 shows the x_1 and x_2 distributions using the reconstructed dijet events from the embedded simulation for the most asymmetric collisions (topology A) in the region $12 < M_{inv} < 14$ GeV/c^2. Figure 4 corresponds to the lowest momentum fraction values probed in these studies. The obtained values of x_1 and x_2 are weighted by the partonic asymmetry to indicate the region that is sensitive to the double-helicity measurement. The dijet triggers were introduced in this analysis specifically to enhance statistics at low x; sacrificing statistics at low p_T for the inclusive jet measurement, as seen in Fig. 3, while providing an order of magnitude greater statistics
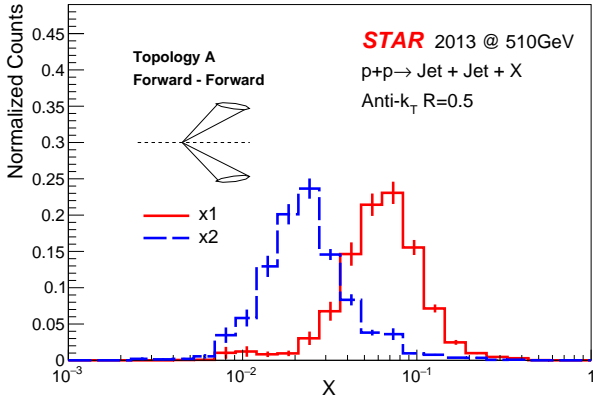
FIG. 4. Sampled x_1 (solid) and x_2 (dashed) gluon distributions weighted by the partonic asymmetry for dijet events with detector level M_{inv} in the range $12 < M_{inv} < 14 \,\mathrm{GeV}/c^2$, obtained using the embedded simulation for the topology A (the most asymmetric collisions). A representation of the topological configuration relative to the beam line is shown.

for the lower M_{inv} bins for the dijet results.

Figure 5 shows the dijet A_{LL} as a function of the parton level invariant mass for the four topologies. Systematic uncertainties for dijet A_{LL} were estimated following the same procedure as used for inclusive jet A_{LL}. The 2012 results [10] and the expectations from global analyses are also shown. Similar to the inclusive jet results, there is good agreement between these and previous dijet results and with the global fits for all topologies.

There are point-to-point correlations between inclusive jet and dijet measurements from systematic effects, in addition to statistical correlations originating from the fact that ∼32% of dijet events included at least one jet from the inclusive measurement. The underlying event and trigger bias systematic uncertainties were treated as fully correlated in A_{LL}. Events with two reconstructed jets, both satisfying the inclusive jet conditions, will also introduce statistical correlations for the inclusive jet measurement. Total correlation matrices were calculated as in [10, 11] for inclusive-inclusive and inclusive-dijet events, and the systematic correlation matrices were calculated for dijet-dijet events (there is no statistical correlation for dijet A_{LL}). Correlation matrices are presented in the supplemental materials [32].

In summary, we report a high precision measurement of the inclusive jet and dijet longitudinal double-spin asymmetry A_{LL} in polarized proton collisions at $\sqrt{s} = 510$ GeV and $|\eta| < 0.9$, using the large data set collected by STAR in 2013. The results are consistent with previous STAR measurements and expectations from the latest global analyses, which included published RHIC data [2, 4, 5]. The inclusive jet results will provide valuable new constraints on the magnitude of the gluon polarization, whereas the dijet results will have an impact on
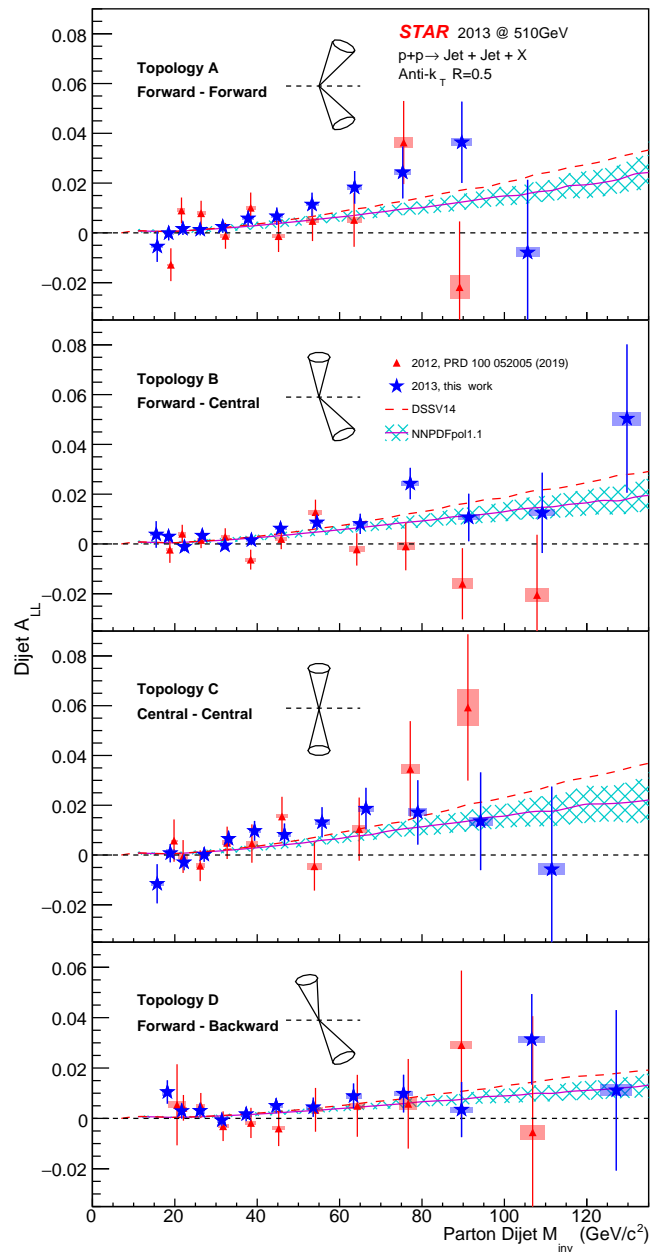
FIG. 5. Dijet A_{LL} versus M_{inv} for the A, B, C and D (top to bottom) topological configurations as explained in the text. They are compared to previous STAR results from 2012 data [10] and predictions from DSSV14 [4] and NNPDFpol1.1 (with its uncertainty) [5] global analyses. The vertical lines are statistical uncertainties. The boxes show the size of the estimated systematic uncertainties. Topological configurations are shown for each jet orientation relative to the beam line. Scale uncertainties from polarization (not shown) are ±6.6% and ±6.4% for 2012 and 2013, respectively.

its functional form, in particular by using the topological configuration A that provides more precise data at low dijet invariant mass. These results provide sensitivity down to $x \sim 0.015$, extending the kinematic coverage in future global analyses.

[1] C. A. Aidala, S. D. Bass, D. Hasch, and G. K. Mallot, Rev. Mod. Phys. **85**, 655 (2013).

[2] L. Adamczyk *et al.* (STAR), Phys. Rev. Lett. **115**, 092002 (2015).

[3] L. Adamczyk *et al.* (STAR), Phys. Rev. D **95**, 071103 (2017).

[4] D. de Florian, R. Sassot, M. Stratmann, and W. Vogelsang, Phys. Rev. Lett. **113**, 012001 (2014).

[5] E. R. Nocera, R. D. Ball, S. Forte, G. Ridolfi, and J. Rojo (NNPDF), Nucl. Phys. B **887**, 276 (2014).

[6] M. Stratmann, in *14th International Workshop on Deep Inelastic Scattering* (2006) pp. 715–718.

[7] The kinematics of the initial partons and final jets are denoted by subscripts 1,2 and 3,4, respectively.

[8] J. Adam *et al.* (STAR), Phys. Rev. D **98**, 032011 (2018).

[9] D. De Florian, G. A. Lucero, R. Sassot, M. Stratmann, and W. Vogelsang, Phys. Rev. D **100**, 114027 (2019).

[10] J. Adam *et al.* (STAR), Phys. Rev. D **100**, 052005 (2019).

[11] M. S. Abdallah *et al.* (STAR), Phys. Rev. D **103**, L091103 (2021).

[12] A. Adare *et al.* (PHENIX), Phys. Rev. D **93**, 011501 (2016).

[13] U. A. Acharya *et al.* (PHENIX), Phys. Rev. D **102**, 032001 (2020).

[14] J. Adam *et al.* (STAR), Phys. Rev. D **98**, 032013 (2018).

[15] O. Jinnouchi *et al.*, in *16th International Spin Physics Symposium (SPIN 2004)* (2004) pp. 515–518.

[16] H. Okada *et al.*, Phys. Lett. B **638**, 450 (2006).

[17] W. Schmidke *et al.*, "RHIC Polarization for Runs 9-17," https://technotes.bnl.gov/PDF?publicationId=209057 (2018).

[18] M. Anderson *et al.*, Nucl. Instrum. Meth. A **499**, 659 (2003).

[19] M. Beddo *et al.* (STAR), Nucl. Instrum. Meth. A **499**, 725 (2003).

[20] C. E. Allgower *et al.* (STAR), Nucl. Instrum. Meth. A **499**, 740 (2003).

[21] W. Llope *et al.*, Nucl. Instrum. Meth. A **759**, 23 (2014).

[22] C. Adler, A. Denisov, E. Garcia, M. J. Murray, H. Strobele, and S. N. White, Nucl. Instrum. Meth. A **470**, 488 (2001).

[23] E. G. Judd *et al.*, Nucl. Instrum. Meth. A **902**, 228 (2018).

[24] M. Cacciari, G. P. Salam, and G. Soyez, JHEP **04**, 063 (2008).

[25] M. Cacciari, G. P. Salam, and G. Soyez, Eur. Phys. J. C **72**, 1896 (2012).

[26] B. B. Abelev *et al.* (ALICE), Phys. Rev. D **91**, 112012 (2015).

[27] T. Sjostrand, S. Mrenna, and P. Z. Skands, JHEP **05**, 026 (2006).

[28] P. Z. Skands, Phys. Rev. D **82**, 074018 (2010), arXiv:1005.3457v5 [hep-ph].

[29] J. Adams *et al.* (STAR), Phys. Lett. B **637**, 161 (2006).

[30] G. Agakishiev *et al.* (STAR), Phys. Rev. Lett. **108**, 072302 (2012).

[31] R. Brun, F. Bruyant, F. Carminati, S. Giani, M. Maire, A. McPherson, G. Patrick, and L. Urban, CERN-W5013, CERN-W-5013, W5013, W-5013 (1994), 10.17181/CERN.MUHF.DMJ1.

[32] See Supplemental Material at [URL will be inserted by publisher] for tables of results, uncertainties, and correlation matrices.

Longitudinal double-spin asymmetry for inclusive jet and dijet production in polarized proton collisions at $\sqrt{s} = 510$ GeV
Supplementary Material

STAR Collaboration

List of Tables

1 Jet energy scale systematic uncertainties

The tables below summarize the results of all the jet energy scale systematic uncertainties considered, the p_T or M_{inv} bin used at detector level, the neutral energy fraction (R_{EM}), the average jet p_T or M_{inv} within the bin used at detector level and the correction factor (δp_T or δM_{inv} in the tables) to unfold the measured results to the parton level. The final systematic uncertainty is the addition in quadrature of all the systematic uncertainties described below. Table 1 summarizes the results of the jet energy scale systematics calculated for inclusive jets. Tables 2, 3, 4 and 5 summarize the results of the jet energy scale systematic uncertainties calculated for dijets in each topology.

1.1 Parton shift error

The statistical errors of each δp_T or δM_{inv} correction, obtained after the bin-by-bin unfolding, are considered as a systematic. See Section V. C. 1. of [10].

1.2 TPC tracking efficiency (hadronic response)

The TPC tracking efficiency or hadronic response (Hadron resp. in the tables) is another systematic related to the detector response uncertainties calculated as described in Section V. C. 1. of [10]. In addition to the main simulation embedding sample, another simulation at the jet tree level was generated by randomly rejecting 4% of the reconstructed tracks to simulate a loss on track reconstruction efficiency as in [11]. The difference between this 4% track loss sample and the nominal embedding sample is considered as a systematic uncertainty, with an additional 1% component added in quadrature, associated with the efficiency of GEANT to simulate the EMCs response of charged hadrons.

1.3 EMC calibration and efficiency (electromagnetic response)

The systematic uncertainty related to the electromagnetic response of BEMC (EM resp.) are quantified by the quadrature sum of BEMC neutral energy uncertainty plus the track efficiency for both TPC and BEMC. For the 2013 data, the BEMC tower gain uncertainty was estimated to be 5% and the track efficiency was estimated to be 1% (same as in [10]). See Section V. C. 1. of [10].

1.4 Underlying event

The systematic uncertainty related to underlying event (UE syst.) corresponds to the average difference of the correcred for UE p_T or M_{inv} between data and embedded simulation within each p_T or M_{inv} bins. See Section V. C. 2. of [10].

1.5 Pythia tune

The quadrature sum of the differences between other Pythia tunes and the nominal tune (370), as it was done for the run 2012 [10] and run 2015 [11] measurements, is considered as a systematic uncertainty (Tune syst.). See Section V. C. 3. of [10].

Detector jet				Hadron resp.	EM resp.	UE syst.	Tune syst.	Parton jet
p_T range	R_{EM}	$\langle p_T \rangle$	δp_T					p_T (final)
$7.0-8.2$	0.67	7.59	0.20 ± 0.21	0.06	0.27	0.05	0.78	7.79 ± 0.86
$8.2-9.6$	0.64	8.81	0.81 ± 0.06	0.07	0.31	0.01	0.49	9.62 ± 0.59
$9.6-11.2$	0.66	10.35	1.32 ± 0.05	0.12	0.37	0.02	0.26	11.67 ± 0.47
$11.2-13.1$	0.63	12.04	1.55 ± 0.05	0.09	0.42	0.03	0.27	13.59 ± 0.51
$13.1-15.3$	0.58	14.05	1.71 ± 0.04	0.18	0.47	0.04	0.19	15.76 ± 0.54
$15.3-17.9$	0.72	16.58	3.31 ± 0.05	0.19	0.63	0.10	0.28	19.89 ± 0.73
$17.9-20.9$	0.69	19.27	3.41 ± 0.04	0.13	0.71	0.09	0.35	22.68 ± 0.81
$20.9-24.5$	0.64	22.49	3.45 ± 0.04	0.20	0.79	0.09	0.35	25.94 ± 0.89
$24.5-28.7$	0.59	26.30	3.45 ± 0.04	0.19	0.88	0.09	0.43	29.75 ± 1.00
$28.7-33.6$	0.55	30.75	3.54 ± 0.04	0.26	1.00	0.11	0.63	34.29 ± 1.21
$33.6-39.3$	0.52	35.94	3.65 ± 0.05	0.30	1.14	0.11	0.74	39.59 ± 1.40
$39.3-46.0$	0.51	41.99	3.77 ± 0.06	0.26	1.32	0.11	0.70	45.76 ± 1.52
$46.0-53.8$	0.50	49.04	4.13 ± 0.08	0.34	1.53	0.11	0.71	53.17 ± 1.73
$53.8-62.8$	0.51	57.21	4.16 ± 0.12	0.27	1.80	0.10	0.68	61.37 ± 1.95

Table 1: Jet energy scale correction and systematic uncertainties for inclusive jets. All values are given in GeV/c.

Detector jet				Hadron resp.	EM resp.	UE syst.	Tune syst.	Parton jet
M_{inv} range	R_{EM}	$\langle M_{inv}\rangle$	δM_{inv}					M_{inv} (final)
12 - 14	0.58	13.30	2.44 ± 0.46	0.61	0.44	0.07	1.19	15.74 ± 1.42
14 - 17	0.56	15.63	2.87 ± 0.20	0.11	0.51	0.10	0.57	18.50 ± 1.14
17 - 20	0.55	18.47	3.49 ± 0.18	0.40	0.60	0.08	0.54	21.96 ± 0.95
20 - 24	0.54	21.84	4.33 ± 0.13	0.41	0.70	0.13	0.44	26.17 ± 0.94
24 - 29	0.52	26.24	5.39 ± 0.11	0.47	0.83	0.13	0.49	31.63 ± 1.04
29 - 34	0.52	31.24	6.56 ± 0.12	0.46	0.99	0.18	0.83	37.80 ± 1.36
34 - 41	0.51	37.04	7.71 ± 0.13	0.54	1.17	0.17	0.58	44.75 ± 1.35
41 - 49	0.50	44.40	8.91 ± 0.14	0.66	1.39	0.24	0.42	53.31 ± 1.50
49 - 59	0.49	53.12	10.52 ± 0.17	0.68	1.65	0.21	0.35	63.64 ± 1.73
59 - 70	0.48	63.50	11.82 ± 0.24	0.97	1.96	0.25	0.53	75.32 ± 2.06
70 - 84	0.47	75.47	14.19 ± 0.28	0.99	2.32	0.26	0.89	89.66 ± 2.51
84 - 101	0.46	90.39	15.24 ± 0.40	1.29	2.76	0.23	0.79	105.63 ± 2.90
101 - 121	-	-	-	-	-	-	-	-

Table 2: Jet energy scale correction and systematic uncertainties for dijets topology A. All values are given in GeV/c^2.

Detector jet								Parton jet
M_{inv} range	R_{EM}	$\langle M_{inv}\rangle$	δM_{inv}	Hadron resp.	EM resp.	UE syst.	Tune syst.	M_{inv} (final)
12 - 14	0.59	13.38	2.11 ± 0.70	0.67	0.45	0.15	1.00	15.49 ± 1.47
14 - 17	0.58	15.68	2.80 ± 0.22	0.22	0.52	0.06	0.57	18.48 ± 0.83
17 - 20	0.57	18.49	3.84 ± 0.13	0.14	0.61	0.05	0.39	22.33 ± 0.75
20 - 24	0.55	21.87	4.80 ± 0.09	0.09	0.71	0.12	0.54	26.67 ± 0.91
24 - 29	0.54	26.25	5.91 ± 0.08	0.08	0.84	0.14	0.48	32.16 ± 0.99
29 - 34	0.53	31.25	7.34 ± 0.09	0.09	1.00	0.20	0.57	38.59 ± 1.17
34 - 41	0.53	37.06	8.60 ± 0.08	0.08	1.18	0.20	0.73	45.66 ± 1.41
41 - 49	0.52	44.43	10.06 ± 0.10	0.10	1.41	0.21	0.49	54.49 ± 1.51
49 - 59	0.50	53.16	11.86 ± 0.12	0.12	1.66	0.23	0.45	65.02 ± 1.75
59 - 70	0.50	63.53	13.63 ± 0.16	0.16	1.99	0.27	0.46	77.16 ± 2.07
70 - 84	0.49	75.58	15.75 ± 0.19	0.19	2.35	0.26	0.97	91.33 ± 2.57
84 - 101	0.49	90.61	18.59 ± 0.25	0.25	2.82	0.26	1.09	109.20 ± 3.05
101 - 121	0.48	108.55	21.20 ± 0.35	0.35	3.35	0.23	0.58	129.75 ± 3.45

Table 3: Jet energy scale correction and systematic uncertainties for dijets topology B. All values are given in GeV/c^2.

Detector jet				Hadron resp.	EM resp.	UE syst.	Tune syst.	Parton jet
M_{inv} range	R_{EM}	$\langle M_{inv}\rangle$	δM_{inv}					M_{inv} (final)
12 - 14	0.59	13.30	2.42 ± 0.72	0.14	0.45	0.03	1.28	15.72 ± 1.54
14 - 17	0.58	15.62	3.28 ± 0.28	0.10	0.52	0.07	0.79	18.90 ± 0.99
17 - 20	0.57	18.47	3.77 ± 0.38	0.38	0.61	0.03	0.61	22.24 ± 1.02
20 - 24	0.56	21.84	5.30 ± 0.16	0.33	0.71	0.17	0.54	27.14 ± 0.98
24 - 29	0.55	26.24	6.79 ± 0.13	0.38	0.85	0.17	0.52	33.03 ± 1.09
29 - 34	0.54	31.25	8.10 ± 0.16	0.46	1.01	0.20	0.87	39.35 ± 1.43
34 - 41	0.53	37.04	9.58 ± 0.16	0.64	1.18	0.23	0.70	46.62 ± 1.54
41 - 49	0.52	44.41	11.33 ± 0.18	0.70	1.41	0.24	0.60	55.74 ± 1.71
49 - 59	0.51	53.15	13.24 ± 0.22	0.82	1.67	0.24	0.40	66.39 ± 1.93
59 - 70	0.50	63.52	15.45 ± 0.29	0.91	1.99	0.29	0.40	78.97 ± 2.26
70 - 84	0.50	75.57	18.65 ± 0.35	1.06	2.36	0.21	1.10	94.22 ± 2.85
84 - 101	0.49	90.54	20.94 ± 0.48	1.29	2.81	0.29	0.70	111.48 ± 3.22
101 - 121	-	-	-	-	-	-	-	-

Table 4: Jet energy scale correction and systematic uncertainties for dijets topology C. All values are given in GeV/c^2.

	Detector jet							Parton jet
M_{inv} range	R_{EM}	$\langle M_{inv} \rangle$	δM_{inv}	Hadron resp.	EM resp.	UE syst.	Tune syst.	M_{inv} (final)
12 - 14	-	-	-	-	-	-	-	-
14 - 17	0.57	15.87	2.33 ± 0.37	0.33	0.52	0.03	0.90	18.20 ± 1.15
17 - 20	0.56	18.56	3.11 ± 0.23	0.36	0.61	0.05	0.72	21.67 ± 1.04
20 - 24	0.55	21.96	4.16 ± 0.16	0.39	0.71	0.08	0.62	26.12 ± 1.04
24 - 29	0.53	26.30	5.12 ± 0.13	0.41	0.84	0.07	0.38	31.42 ± 1.02
29 - 34	0.52	31.27	6.06 ± 0.14	0.45	0.99	0.16	0.57	37.33 ± 1.25
34 - 41	0.51	37.10	7.50 ± 0.14	0.51	1.17	0.16	0.78	44.60 ± 1.51
41 - 49	0.51	44.48	9.13 ± 0.15	0.59	1.40	0.21	0.69	53.61 ± 1.69
49 - 59	0.50	53.21	10.17 ± 0.18	0.70	1.66	0.21	0.62	63.38 ± 1.93
59 - 70	0.49	63.60	11.92 ± 0.22	0.86	1.98	0.22	0.66	75.52 ± 2.27
70 - 84	0.48	75.62	13.98 ± 0.28	1.10	2.34	0.30	0.65	89.60 ± 2.70
84 - 101	0.47	90.73	15.90 ± 0.37	1.00	2.79	0.24	1.13	106.63 ± 3.20
101 - 121	0.47	108.76	18.41 ± 0.48	1.42	3.34	0.27	1.07	127.17 ± 3.82

Table 5: Jet energy scale correction and systematic uncertainties for dijets topology D. All values are given in GeV/c^2.

2 Asymmetry corrections and systematic errors

Tables 6, 7, 8, 9 and 10 summarize the results of the asymmetry corrections and systematic uncertainties calculated for inclusive jets and dijets in each topology. The total A_{LL} systematic uncertainties are the quadrature sum of the trigger and reconstruction bias, the underlying event uncertainty, and the relative luminosity uncertainty, estimated to be 4.7×10^{-4}.

2.1 Trigger and Reconstruction bias

The trigger bias correction values were calculated from the average difference between the reconstructed detector jets i.e., the bias sample (from the embedded simulation) and parton jets obtained by using one hundred equally probable A_{LL} replicas of the NNPDF pol1.1 [5] estimations. The root-mean-square of these differences (Corr Err in the tables) and the finite statistics of the simulation (Stat Err in the tables) are considered as systematic uncertainties, related to the PDF used, for the inclusive jet and dijet A_{LL} results. See Section V. D. 3. of [10].

2.2 UE asymmetry systematics

The underlying event systematics (UE syst in the tables) were calculated according to Section V. D. 1. of [10].

p_T range (GeV/c)	Correction	Corr Err	Stat Err	UE syst	Total A_{LL} Syst
$7.0 - 8.2$	-0.00035	0.00017	0.00005	0.00033	0.00060
$8.2 - 9.6$	-0.00034	0.00013	0.00006	0.00027	0.00056
$9.6 - 11.2$	-0.00033	0.00009	0.00005	0.00024	0.00054
$11.2 - 13.1$	-0.00038	0.00010	0.00007	0.00020	0.00053
$13.1 - 15.3$	-0.00037	0.00010	0.00006	0.00017	0.00051
$15.3 - 17.9$	-0.00013	0.00007	0.00006	0.00016	0.00050
$17.9 - 20.9$	-0.00020	0.00008	0.00007	0.00014	0.00050
$20.9 - 24.5$	-0.00016	0.00014	0.00009	0.00012	0.00051
$24.5 - 28.7$	-0.00039	0.00022	0.00012	0.00010	0.00054
$28.7 - 33.6$	-0.00020	0.00031	0.00017	0.00009	0.00059
$33.6 - 39.3$	-0.00026	0.00036	0.00023	0.00008	0.00064
$39.3 - 46.0$	-0.00025	0.00034	0.00034	0.00007	0.00068
$46.0 - 53.8$	-0.00106	0.00060	0.00051	0.00006	0.00092
$53.8 - 62.8$	-0.00018	0.00190	0.00081	0.00006	0.00212

Table 6: Asymmetry correction and systematic uncertainties for inclusive jets.

M_{inv} range (GeV/c^2)	Correction	Corr Err	Stat Err	UE syst	Total A_{LL} Syst
12 - 14	0.00008	0.00013	0.00010	0.00023	0.00055
14 - 17	-0.00007	0.00008	0.00007	0.00056	0.00074
17 - 20	-0.00018	0.00011	0.00010	0.00006	0.00050
20 - 24	-0.00032	0.00015	0.00011	0.00022	0.00055
24 - 29	-0.00036	0.00021	0.00013	0.00019	0.00056
29 - 34	-0.00042	0.00022	0.00018	0.00015	0.00057
34 - 41	-0.00046	0.00025	0.00023	0.00013	0.00059
41 - 49	-0.00056	0.00031	0.00032	0.00011	0.00066
49 - 59	0.00010	0.00045	0.00049	0.00010	0.00082
59 - 70	-0.00104	0.00065	0.00080	0.00008	0.00114
70 - 84	-0.00148	0.00083	0.00107	0.00007	0.00144
84 - 101	-0.00115	0.00084	0.00173	0.00007	0.00198
101 - 121	-	-	-	-	-

Table 7: Asymmetry correction and systematic uncertainties for dijets topology A.

M_{inv} range (GeV/c^2)	Correction	Corr Err	Stat Err	UE syst	Total A_{LL} Syst
12 - 14	-0.00005	0.00008	0.00007	0.00004	0.00048
14 - 17	-0.00003	0.00008	0.00005	0.00005	0.00048
17 - 20	-0.00007	0.00009	0.00007	0.00001	0.00048
20 - 24	-0.00026	0.00012	0.00007	0.00003	0.00049
24 - 29	-0.00041	0.00017	0.00008	0.00003	0.00051
29 - 34	-0.00041	0.00021	0.00011	0.00002	0.00053
34 - 41	-0.00047	0.00026	0.00014	0.00002	0.00056
41 - 49	-0.00053	0.00034	0.00021	0.00002	0.00062
49 - 59	-0.00109	0.00048	0.00030	0.00001	0.00074
59 - 70	-0.00031	0.00067	0.00047	0.00001	0.00094
70 - 84	-0.00082	0.00073	0.00065	0.00001	0.00108
84 - 101	0.00063	0.00060	0.00094	0.00001	0.00121
101 - 121	-0.00162	0.00232	0.00149	0.00001	0.00280

Table 8: Asymmetry correction and systematic uncertainties for dijets topology B.

M_{inv} range (GeV/c^2)	Correction	Corr Err	Stat Err	UE syst	Total A_{LL} Syst
12 - 14	0.00003	0.00012	0.00018	0.00060	0.00079
14 - 17	0.00004	0.00010	0.00010	0.00145	0.00153
17 - 20	-0.00011	0.00012	0.00011	0.00015	0.00052
20 - 24	-0.00029	0.00014	0.00012	0.00056	0.00075
24 - 29	-0.00021	0.00018	0.00016	0.00047	0.00071
29 - 34	0.00023	0.00025	0.00023	0.00040	0.00070
34 - 41	-0.00042	0.00031	0.00031	0.00034	0.00073
41 - 49	-0.00044	0.00042	0.00044	0.00029	0.00082
49 - 59	-0.00020	0.00062	0.00066	0.00026	0.00105
59 - 70	0.00045	0.00097	0.00103	0.00021	0.00151
70 - 84	0.00012	0.00089	0.00139	0.00018	0.00173
84 - 101	-0.00297	0.00105	0.00205	0.00015	0.00236
101 - 121	-	-	-	-	-

Table 9: Asymmetry correction and systematic uncertainties for dijets topology C.

M_{inv} range (GeV/c^2)	Correction	Corr Err	Stat Err	UE syst	Total A_{LL} Syst
12 - 14	-	-	-	-	-
14 - 17	-0.00014	0.00012	0.00008	0.00110	0.00120
17 - 20	-0.00010	0.00010	0.00008	0.00025	0.00055
20 - 24	-0.00037	0.00013	0.00009	0.00102	0.00113
24 - 29	-0.00043	0.00016	0.00009	0.00083	0.00097
29 - 34	-0.00055	0.00020	0.00013	0.00068	0.00086
34 - 41	-0.00069	0.00023	0.00017	0.00060	0.00081
41 - 49	-0.00068	0.00027	0.00025	0.00054	0.00080
49 - 59	-0.00054	0.00040	0.00034	0.00041	0.00082
59 - 70	-0.00119	0.00053	0.00051	0.00036	0.00094
70 - 84	-0.00093	0.00055	0.00071	0.00031	0.00106
84 - 101	-0.00063	0.00042	0.00102	0.00028	0.00123
101 - 121	-0.00006	0.00159	0.00149	0.00024	0.00224

Table 10: Asymmetry correction and systematic uncertainties for dijets topology D.

3   2013 STAR Results

Table 11 presents the numerical results of the analysis for inclusive jets. Tables 12 and 13 present the results of the run 2013 analysis for each topology of the dijets.

p_T bin	Jet p_T	$A_{LL} \pm$ stat. $\pm$ syst.
$7.0 - 8.2$	7.79 ± 0.86	$0.00626 \pm 0.00241 \pm 0.00060$
$8.2 - 9.6$	9.62 ± 0.59	$0.00258 \pm 0.00249 \pm 0.00056$
$9.6 - 11.2$	11.67 ± 0.47	$0.00277 \pm 0.00176 \pm 0.00054$
$11.2 - 13.1$	13.59 ± 0.51	$-0.00075 \pm 0.00187 \pm 0.00054$
$13.1 - 15.3$	15.76 ± 0.54	$-0.00085 \pm 0.00216 \pm 0.00051$
$15.3 - 17.9$	19.89 ± 0.73	$0.00444 \pm 0.00112 \pm 0.00050$
$17.9 - 20.9$	22.68 ± 0.81	$0.00308 \pm 0.00114 \pm 0.00050$
$20.9 - 24.5$	25.94 ± 0.89	$0.00572 \pm 0.00128 \pm 0.00051$
$24.5 - 28.7$	29.75 ± 1.00	$0.01008 \pm 0.00161 \pm 0.00054$
$28.7 - 33.6$	34.29 ± 1.21	$0.01033 \pm 0.00217 \pm 0.00059$
$33.6 - 39.3$	39.59 ± 1.40	$0.01249 \pm 0.00312 \pm 0.00064$
$39.3 - 46.0$	45.76 ± 1.52	$0.01824 \pm 0.00478 \pm 0.00068$
$46.0 - 53.8$	53.17 ± 1.73	$0.02205 \pm 0.00788 \pm 0.00092$
$53.8 - 62.8$	61.37 ± 1.95	$0.04527 \pm 0.01388 \pm 0.00212$

Table 11: Inclusive jet A_{LL} results.

M_{inv} bin	Dijet M_{inv}	$A_{LL} \pm$ stat. $\pm$ syst.
Topology A: Forward-Forward Dijets		
12 - 14	15.74 ± 1.42	-0.00548 ± 0.00619 ± 0.00055
14 - 17	18.50 ± 1.14	-0.00011 ± 0.00289 ± 0.00074
17 - 20	21.96 ± 0.95	0.00165 ± 0.00248 ± 0.00050
20 - 24	26.17 ± 0.94	0.00129 ± 0.00226 ± 0.00055
24 - 29	31.63 ± 1.04	0.00248 ± 0.00246 ± 0.00056
29 - 34	37.80 ± 1.36	0.00581 ± 0.00311 ± 0.00057
34 - 41	44.75 ± 1.35	0.00666 ± 0.00349 ± 0.00059
41 - 49	53.31 ± 1.50	0.01140 ± 0.00472 ± 0.00066
49 - 59	63.64 ± 1.73	0.01826 ± 0.00659 ± 0.00082
59 - 70	75.32 ± 2.06	0.02431 ± 0.01045 ± 0.00114
70 - 84	89.66 ± 2.51	0.03638 ± 0.01633 ± 0.00144
84 - 101	105.63 ± 2.90	-0.00789 ± 0.02919 ± 0.00198
101 - 121	-	-
Topology B: Forward-Central Dijets		
12 - 14	15.49 ± 1.47	0.00381 ± 0.00533 ± 0.00048
14 - 17	18.48 ± 0.83	0.00299 ± 0.00213 ± 0.00048
17 - 20	22.33 ± 0.75	-0.00116 ± 0.00173 ± 0.00048
20 - 24	26.67 ± 0.91	0.00336 ± 0.00152 ± 0.00049
24 - 29	32.16 ± 0.99	-0.00060 ± 0.00161 ± 0.00051
29 - 34	38.59 ± 1.17	0.00154 ± 0.00202 ± 0.00053
34 - 41	45.66 ± 1.41	0.00620 ± 0.00224 ± 0.00056
41 - 49	54.49 ± 1.51	0.00865 ± 0.00297 ± 0.00062
49 - 59	65.02 ± 1.75	0.00806 ± 0.00406 ± 0.00074
59 - 70	77.16 ± 2.07	0.02428 ± 0.00629 ± 0.00094
70 - 84	91.33 ± 2.57	0.01063 ± 0.00953 ± 0.00108
84 - 101	109.20 ± 3.05	0.01248 ± 0.01613 ± 0.00121
101 - 121	129.75 ± 3.45	0.05037 ± 0.02978 ± 0.00280

Table 12: Dijet A_{LL} results for topologies A and B.

M_{inv} bin	Dijet M_{inv}	$A_{LL} \pm$ stat. $\pm$ syst.
Topology C: Central-Central Dijets		
12 - 14	15.72 ± 1.54	-0.01155 ± 0.00785 ± 0.00079
14 - 17	18.90 ± 0.99	0.00075 ± 0.00367 ± 0.00153
17 - 20	22.24 ± 1.02	-0.00293 ± 0.00317 ± 0.00052
20 - 24	27.14 ± 0.98	0.00018 ± 0.00291 ± 0.00075
24 - 29	33.03 ± 1.09	0.00655 ± 0.00317 ± 0.00071
29 - 34	39.35 ± 1.43	0.00969 ± 0.00400 ± 0.00070
34 - 41	46.62 ± 1.54	0.00817 ± 0.00448 ± 0.00073
41 - 49	55.74 ± 1.71	0.01317 ± 0.00603 ± 0.00082
49 - 59	66.39 ± 1.93	0.01866 ± 0.00833 ± 0.00105
59 - 70	78.97 ± 2.26	0.01712 ± 0.01292 ± 0.00151
70 - 84	94.22 ± 2.85	0.01357 ± 0.01964 ± 0.00173
84 - 101	111.48 ± 3.22	-0.00575 ± 0.03322 ± 0.00236
101 - 121	-	-
Topology D: Forward-Backward Dijets		
12 - 14	-	-
14 - 17	18.20 ± 1.15	0.01048 ± 0.00466 ± 0.00120
17 - 20	21.67 ± 1.04	0.00296 ± 0.00302 ± 0.00055
20 - 24	26.12 ± 1.04	0.00307 ± 0.00235 ± 0.00113
24 - 29	31.42 ± 1.02	-0.00072 ± 0.00229 ± 0.00097
29 - 34	37.33 ± 1.25	0.00169 ± 0.00278 ± 0.00086
34 - 41	44.60 ± 1.51	0.00501 ± 0.00300 ± 0.00081
41 - 49	53.61 ± 1.69	0.00443 ± 0.00382 ± 0.00080
49 - 59	63.38 ± 1.93	0.00887 ± 0.00500 ± 0.00082
59 - 70	75.52 ± 2.27	0.00985 ± 0.00747 ± 0.00094
70 - 84	89.60 ± 2.70	0.00351 ± 0.01095 ± 0.00106
84 - 101	106.63 ± 3.20	0.03141 ± 0.01797 ± 0.00123
101 - 121	127.17 ± 3.82	0.01114 ± 0.03187 ± 0.00224

Table 13: Dijet A_{LL} results for topologies C and D.

4 Correlation Matrices

Table 14 shows the binning and the labels of the inclusive jet results, to represent the correlation matrices. Table 15 shows the binning and the labels of the dijet results for each topology, to represent the correlation matrices. The last bins (101 - 121 GeV/c^2) for topologies A and C, and the first bin (12 - 14 GeV/c^2) of topology D, are not included due to poor statistics (*). The relative luminosity uncertainty (4.7×10^{-4}) and the beam polarization uncertainty ($\pm 6.4\%$), which are common to all the data points, were not included in the calculations.

Range (GeV/c)	Label
7.0 - 8.2	I1
8.2 - 9.6	I2
9.6 - 11.2	I3
11.2 - 13.1	I4
13.1 - 15.3	I5
15.3 - 17.9	I6
17.9 - 21.0	I7
21.0 - 24.5	I8
24.5 - 28.7	I9
28.7 - 33.6	I10
33.6 - 39.3	I11
39.3 - 45.9	I12
45.9 - 53.7	I13
53.7 - 62.8	I14

Table 14: Inclusive jet bins and labels for correlation matrices.

Range (GeV/c^2)	Topology A	Topology B	Topology C	Topology D
12 - 14	A1	B1	C1	D1*
14 - 17	A2	B2	C2	D2
17 - 20	A3	B3	C3	D3
20 - 24	A4	B4	C4	D4
24 - 29	A5	B5	C5	D5
29 - 34	A6	B6	C6	D6
34 - 41	A7	B7	C7	D7
41 - 49	A8	B8	C8	D8
49 - 59	A9	B9	C9	D9
59 - 70	A10	B10	C10	D10
70 - 84	A11	B11	C11	D11
84 -101	A12	B12	C12	D12
101 -121	A13*	B13	C13*	D13

Table 15: Dijet bins and labels in each topology for correlation matrices.

Labels	I1	I2	I3	I4	I5	I6	I7	I8	I9	I10	I11	I12	I13	I14
7.0 - 8.2	1	0.007	0.004	0.004	0.003	0.001	0.001	0.000	0.000	0.000	0.000	0.000	0.000	0.000
8.2 - 9.6		1	0.005	0.005	0.005	0.002	0.001	0.001	0.000	0.000	0.000	0.000	0.000	0.000
9.6 - 11.2			1	0.008	0.009	0.004	0.002	0.002	0.001	0.001	0.000	0.000	0.000	0.000
11.2 - 13.1				1	0.012	0.005	0.004	0.002	0.002	0.001	0.000	0.000	0.000	0.000
13.1 - 15.3					1	0.007	0.005	0.004	0.003	0.002	0.001	0.000	0.000	0.000
15.3 - 17.9						1	0.009	0.010	0.009	0.007	0.005	0.003	0.002	0.001
17.9 - 21.0							1	0.013	0.013	0.011	0.009	0.005	0.003	0.001
21.0 - 24.5								1	0.019	0.018	0.014	0.010	0.006	0.003
24.5 - 28.7									1	0.024	0.022	0.016	0.010	0.005
28.7 - 33.6										1	0.029	0.025	0.017	0.010
33.6 - 39.3											1	0.033	0.026	0.017
39.3 - 45.9												1	0.036	0.027
45.9 - 53.7													1	0.037
53.7 - 62.8														1

Table 16: The correlation matrix for the point-to-point uncertainties (statistical and systematic) for the inclusive jet measurements. The relative luminosity and beam polarization uncertainties are not included because they are the same for all points.

17

Label	A1	A2	A3	A4	A5	A6	A7	A8	A9	A10	A11	A12	A13*
7.0 - 8.2	0.021	0.012	0.005	0.002	0.000	0.000	0.000	0.000	0.000	0.000	0.000	0.000	-
8.2 - 9.6	0.008	0.017	0.009	0.005	0.002	0.000	0.000	0.000	0.000	0.000	0.000	0.000	-
9.6 - 11.2	0.001	0.022	0.019	0.014	0.007	0.002	0.000	0.000	0.000	0.000	0.000	0.000	-
11.2 - 13.1	0.000	0.010	0.021	0.020	0.015	0.006	0.002	0.000	0.000	0.000	0.000	0.000	-
13.1 - 15.3	0.000	0.001	0.016	0.020	0.020	0.014	0.006	0.001	0.000	0.000	0.000	0.000	-
15.3 - 17.9	0.000	0.000	0.013	0.033	0.047	0.049	0.041	0.017	0.004	0.000	0.000	0.000	-
17.9 - 21.0	0.000	0.000	0.002	0.023	0.041	0.055	0.066	0.045	0.015	0.002	0.000	0.000	-
21.0 - 24.5	0.000	0.000	0.000	0.010	0.027	0.043	0.071	0.077	0.047	0.012	0.001	0.000	-
24.5 - 28.7	0.000	0.000	0.000	0.002	0.014	0.025	0.051	0.081	0.088	0.043	0.009	0.001	-
28.7 - 33.6	0.000	0.000	0.000	0.000	0.004	0.011	0.026	0.055	0.094	0.090	0.039	0.006	-
33.6 - 39.3	0.000	0.000	0.000	0.000	0.000	0.003	0.011	0.027	0.062	0.101	0.094	0.030	-
39.3 - 45.9	0.000	0.000	0.000	0.000	0.000	0.000	0.003	0.010	0.029	0.066	0.114	0.091	-
45.9 - 53.7	0.000	0.000	0.000	0.000	0.000	0.000	0.000	0.002	0.010	0.028	0.071	0.116	-
53.7 - 62.8	0.000	0.000	0.000	0.000	0.000	0.000	0.000	0.000	0.002	0.009	0.028	0.076	-

Table 17: The correlation matrix for the point-to-point uncertainties (statistical and systematic) for the inclusive jet measurements coupling with the forward-forward dijet measurements (Topology A). The relative luminosity and beam polarization uncertainties are not included because they are the same for all points.

Label	B1	B2	B3	B4	B5	B6	B7	B8	B9	B10	B11	B12	B13
7.0 - 8.2	0.026	0.022	0.009	0.004	0.001	0.000	0.000	0.000	0.000	0.000	0.000	0.000	0.000
8.2 - 9.6	0.007	0.025	0.015	0.008	0.003	0.001	0.000	0.000	0.000	0.000	0.000	0.000	0.000
9.6 - 11.2	0.001	0.025	0.029	0.022	0.013	0.005	0.001	0.000	0.000	0.000	0.000	0.000	0.000
11.2 - 13.1	0.000	0.009	0.029	0.029	0.023	0.012	0.004	0.001	0.000	0.000	0.000	0.000	0.000
13.1 - 15.3	0.000	0.001	0.017	0.027	0.029	0.022	0.012	0.003	0.000	0.000	0.000	0.000	0.000
15.3 - 17.9	0.000	0.000	0.010	0.041	0.061	0.068	0.065	0.033	0.009	0.001	0.000	0.000	0.000
17.9 - 21.0	0.000	0.000	0.001	0.025	0.052	0.073	0.095	0.075	0.033	0.007	0.001	0.000	0.000
21.0 - 24.5	0.000	0.000	0.000	0.008	0.033	0.055	0.093	0.112	0.082	0.028	0.005	0.000	0.000
24.5 - 28.7	0.000	0.000	0.000	0.001	0.015	0.031	0.063	0.105	0.129	0.080	0.025	0.003	0.000
28.7 - 33.6	0.000	0.000	0.000	0.000	0.003	0.013	0.033	0.069	0.124	0.136	0.079	0.018	0.001
33.6 - 39.3	0.000	0.000	0.000	0.000	0.000	0.003	0.013	0.033	0.079	0.136	0.149	0.069	0.011
39.3 - 45.9	0.000	0.000	0.000	0.000	0.000	0.000	0.003	0.012	0.037	0.085	0.156	0.152	0.053
45.9 - 53.7	0.000	0.000	0.000	0.000	0.000	0.000	0.000	0.002	0.012	0.038	0.096	0.173	0.144
53.7 - 62.8	0.000	0.000	0.000	0.000	0.000	0.000	0.000	0.000	0.002	0.012	0.040	0.110	0.182

Table 18: The correlation matrix for the point-to-point uncertainties (statistical and systematic) for the inclusive jet measurements coupling with the forward-central dijet measurements (Topology B). The relative luminosity and beam polarization uncertainties are not included because they are the same for all points.

Label	C1	C2	C3	C4	C5	C6	C7	C8	C9	C10	C11	C12	C13*
7.0 - 8.2	0.015	0.009	0.004	0.002	0.000	0.000	0.000	0.000	0.000	0.000	0.000	0.000	-
8.2 - 9.6	0.006	0.012	0.007	0.004	0.001	0.000	0.000	0.000	0.000	0.000	0.000	0.000	-
9.6 - 11.2	0.001	0.015	0.014	0.011	0.006	0.002	0.000	0.000	0.000	0.000	0.000	0.000	-
11.2 - 13.1	0.000	0.007	0.016	0.015	0.012	0.005	0.002	0.000	0.000	0.000	0.000	0.000	-
13.1 - 15.3	0.000	0.001	0.011	0.015	0.016	0.011	0.005	0.001	0.000	0.000	0.000	0.000	-
15.3 - 17.9	0.000	0.000	0.008	0.023	0.033	0.035	0.030	0.013	0.003	0.000	0.000	0.000	-
17.9 - 21.0	0.000	0.000	0.001	0.016	0.030	0.041	0.051	0.034	0.013	0.002	0.000	0.000	-
21.0 - 24.5	0.000	0.000	0.000	0.007	0.020	0.033	0.054	0.059	0.036	0.011	0.002	0.000	-
24.5 - 28.7	0.000	0.000	0.000	0.001	0.009	0.018	0.038	0.061	0.067	0.034	0.009	0.001	-
28.7 - 33.6	0.000	0.000	0.000	0.000	0.003	0.008	0.020	0.042	0.072	0.070	0.033	0.006	-
33.6 - 39.3	0.000	0.000	0.000	0.000	0.000	0.002	0.008	0.021	0.049	0.079	0.075	0.027	-
39.3 - 45.9	0.000	0.000	0.000	0.000	0.000	0.000	0.002	0.008	0.024	0.054	0.090	0.074	-
45.9 - 53.7	0.000	0.000	0.000	0.000	0.000	0.000	0.000	0.002	0.009	0.025	0.062	0.097	-
53.7 - 62.8	0.000	0.000	0.000	0.000	0.000	0.000	0.000	0.000	0.002	0.008	0.028	0.073	-

Table 19: The correlation matrix for the point-to-point uncertainties (statistical and systematic) for the inclusive jet measurements coupling with the central-central dijet measurements (Topology C). The relative luminosity and beam polarization uncertainties are not included because they are the same for all points.

Label	D1*	D2	D3	D4	D5	D6	D7	D8	D9	D10	D11	D12	D13
7.0 - 8.2	-	0.019	0.010	0.004	0.002	0.000	0.000	0.000	0.000	0.000	0.000	0.000	0.000
8.2 - 9.6	-	0.013	0.014	0.008	0.004	0.001	0.000	0.000	0.000	0.000	0.000	0.000	0.000
9.6 - 11.2	-	0.006	0.021	0.017	0.012	0.006	0.002	0.000	0.000	0.000	0.000	0.000	0.000
11.2 - 13.1	-	0.001	0.013	0.019	0.017	0.012	0.006	0.001	0.000	0.000	0.000	0.000	0.000
13.1 - 15.3	-	0.000	0.004	0.015	0.019	0.017	0.013	0.005	0.001	0.000	0.000	0.000	0.000
15.3 - 17.9	-	0.000	0.001	0.016	0.033	0.042	0.050	0.036	0.015	0.003	0.000	0.000	0.000
17.9 - 21.0	-	0.000	0.000	0.006	0.025	0.038	0.058	0.060	0.039	0.013	0.002	0.000	0.000
21.0 - 24.5	-	0.000	0.000	0.001	0.013	0.026	0.048	0.069	0.071	0.038	0.011	0.001	0.000
24.5 - 28.7	-	0.000	0.000	0.000	0.004	0.014	0.029	0.053	0.081	0.076	0.038	0.008	0.000
28.7 - 33.6	-	0.000	0.000	0.000	0.000	0.005	0.014	0.030	0.061	0.089	0.082	0.031	0.005
33.6 - 39.3	-	0.000	0.000	0.000	0.000	0.000	0.004	0.013	0.033	0.066	0.103	0.080	0.025
39.3 - 45.9	-	0.000	0.000	0.000	0.000	0.000	0.001	0.004	0.013	0.035	0.076	0.111	0.073
45.9 - 53.7	-	0.000	0.000	0.000	0.000	0.000	0.000	0.000	0.004	0.013	0.038	0.088	0.114
53.7 - 62.8	-	0.000	0.000	0.000	0.000	0.000	0.000	0.000	0.000	0.003	0.013	0.040	0.096

Table 20: The correlation matrix for the point-to-point uncertainties (statistical and systematic) for the inclusive jet measurements coupling with the forward-backward dijet measurements (Topology D). The relative luminosity and beam polarization uncertainties are not included because they are the same for all points.

Label	A1	A2	A3	A4	A5	A6	A7	A8	A9	A10	A11	A12	A13*
A1	1	0.016	0.019	0.021	0.019	0.015	0.014	0.010	0.007	0.005	0.003	0.002	-
A2		1	0.073	0.079	0.073	0.058	0.052	0.039	0.028	0.017	0.011	0.006	-
A3			1	0.042	0.039	0.031	0.028	0.021	0.015	0.009	0.006	0.003	-
A4				1	0.052	0.041	0.037	0.027	0.020	0.012	0.008	0.004	-
A5					1	0.039	0.035	0.026	0.019	0.012	0.008	0.004	-
A6						1	0.029	0.022	0.015	0.010	0.006	0.004	-
A7							1	0.021	0.015	0.009	0.006	0.003	-
A8								1	0.013	0.008	0.005	0.003	-
A9									1	0.010	0.006	0.003	-
A10										1	0.007	0.004	-
A11											1	0.004	-
A12												1	-
A13													-

Table 21: The correlation matrix for the point-to-point uncertainties (systematic only) for forward-forward dijet measurements (Topology A). The relative luminosity and beam polarization uncertainties are not included because they are the same for all points.

Label	B1	B2	B3	B4	B5	B6	B7	B8	B9	B10	B11	B12	B13
A1	0.008	0.018	0.022	0.024	0.022	0.018	0.016	0.012	0.009	0.006	0.004	0.002	0.001
A2	0.000	0.055	0.065	0.072	0.068	0.054	0.049	0.037	0.027	0.017	0.011	0.006	0.003
A3	0.000	0.000	0.053	0.059	0.055	0.044	0.040	0.030	0.022	0.014	0.009	0.005	0.003
A4	0.000	0.000	0.000	0.073	0.068	0.055	0.049	0.037	0.027	0.017	0.011	0.006	0.003
A5	0.000	0.000	0.000	0.000	0.067	0.054	0.049	0.037	0.026	0.017	0.011	0.006	0.003
A6	0.000	0.000	0.000	0.000	0.000	0.046	0.041	0.031	0.023	0.014	0.009	0.005	0.003
A7	0.000	0.000	0.000	0.000	0.000	0.000	0.040	0.030	0.022	0.014	0.009	0.005	0.003
A8	0.000	0.000	0.000	0.000	0.000	0.000	0.000	0.028	0.020	0.013	0.008	0.005	0.003
A9	0.000	0.000	0.000	0.000	0.000	0.000	0.000	0.000	0.022	0.014	0.009	0.005	0.003
A10	0.000	0.000	0.000	0.000	0.000	0.000	0.000	0.000	0.000	0.016	0.010	0.006	0.003
A11	0.000	0.000	0.000	0.000	0.000	0.000	0.000	0.000	0.000	0.000	0.010	0.006	0.003
A12	0.000	0.000	0.000	0.000	0.000	0.000	0.000	0.000	0.000	0.000	0.000	0.005	0.003
A13*	-	-	-	-	-	-	-	-	-	-	-	-	-

Table 22: The correlation matrix for the point-to-point uncertainties (systematic only) coupling forward-forward dijet measurements (Topology A) with forward-central dijet measurements (Topology B). The relative luminosity and beam polarization uncertainties are not included because they are the same for all points.

Label	C1	C2	C3	C4	C5	C6	C7	C8	C9	C10	C11	C12	C13*
A1	0.009	0.018	0.022	0.023	0.022	0.017	0.015	0.012	0.008	0.005	0.003	0.002	-
A2	0.000	0.096	0.116	0.125	0.115	0.092	0.082	0.061	0.044	0.028	0.018	0.011	-
A3	0.000	0.000	0.032	0.035	0.032	0.025	0.023	0.017	0.012	0.008	0.005	0.003	-
A4	0.000	0.000	0.000	0.059	0.055	0.044	0.039	0.029	0.021	0.013	0.009	0.005	-
A5	0.000	0.000	0.000	0.000	0.049	0.039	0.035	0.026	0.019	0.012	0.008	0.004	-
A6	0.000	0.000	0.000	0.000	0.000	0.031	0.028	0.021	0.015	0.010	0.006	0.004	-
A7	0.000	0.000	0.000	0.000	0.000	0.000	0.027	0.020	0.014	0.009	0.006	0.003	-
A8	0.000	0.000	0.000	0.000	0.000	0.000	0.000	0.018	0.013	0.008	0.006	0.003	-
A9	0.000	0.000	0.000	0.000	0.000	0.000	0.000	0.000	0.015	0.010	0.006	0.004	-
A10	0.000	0.000	0.000	0.000	0.000	0.000	0.000	0.000	0.000	0.012	0.008	0.005	-
A11	0.000	0.000	0.000	0.000	0.000	0.000	0.000	0.000	0.000	0.000	0.008	0.004	-
A12	0.000	0.000	0.000	0.000	0.000	0.000	0.000	0.000	0.000	0.000	0.000	0.005	-
A13*	-	-	-	-	-	-	-	-	-	-	-	-	-

Table 23: The correlation matrix for the point-to-point uncertainties (systematic only) coupling forward-forward dijet measurements (Topology A) with central-central dijet measurements (Topology C). The relative luminosity and beam polarization uncertainties are not included because they are the same for all points.

Label	D1*	D2	D3	D4	D5	D6	D7	D8	D9	D10	D11	D12	D13
A1	-	0.029	0.039	0.044	0.043	0.036	0.033	0.025	0.019	0.012	0.008	0.005	0.003
A2	-	0.062	0.084	0.096	0.094	0.078	0.071	0.054	0.040	0.026	0.017	0.010	0.005
A3	-	0.000	0.035	0.041	0.040	0.033	0.030	0.023	0.017	0.011	0.007	0.004	0.002
A4	-	0.000	0.000	0.105	0.103	0.084	0.077	0.059	0.044	0.029	0.019	0.011	0.006
A5	-	0.000	0.000	0.000	0.088	0.072	0.066	0.051	0.038	0.025	0.016	0.010	0.005
A6	-	0.000	0.000	0.000	0.000	0.054	0.049	0.038	0.028	0.018	0.012	0.007	0.004
A7	-	0.000	0.000	0.000	0.000	0.000	0.044	0.034	0.025	0.016	0.011	0.006	0.003
A8	-	0.000	0.000	0.000	0.000	0.000	0.000	0.028	0.021	0.014	0.009	0.005	0.003
A9	-	0.000	0.000	0.000	0.000	0.000	0.000	0.000	0.020	0.013	0.009	0.005	0.003
A10	-	0.000	0.000	0.000	0.000	0.000	0.000	0.000	0.000	0.013	0.009	0.005	0.003
A11	-	0.000	0.000	0.000	0.000	0.000	0.000	0.000	0.000	0.000	0.008	0.005	0.003
A12	-	0.000	0.000	0.000	0.000	0.000	0.000	0.000	0.000	0.000	0.000	0.005	0.002
A13*	-	-	-	-	-	-	-	-	-	-	-	-	-

Table 24: The correlation matrix for the point-to-point uncertainties (systematic only) coupling forward-forward dijet measurements (Topology A) with forward-backward dijet measurements (Topology D). The relative luminosity and beam polarization uncertainties are not included because they are the same for all points.

Label	B1	B2	B3	B4	B5	B6	B7	B8	B9	B10	B11	B12	B13
B1	1	0.020	0.024	0.027	0.025	0.021	0.019	0.014	0.010	0.007	0.004	0.003	0.001
B2		1	0.059	0.066	0.062	0.051	0.046	0.035	0.026	0.017	0.011	0.007	0.004
B3			1	0.080	0.076	0.061	0.056	0.042	0.031	0.020	0.013	0.008	0.004
B4				1	0.089	0.072	0.065	0.050	0.036	0.024	0.016	0.009	0.005
B5					1	0.074	0.067	0.051	0.037	0.024	0.016	0.010	0.005
B6						1	0.058	0.044	0.033	0.021	0.014	0.008	0.004
B7							1	0.043	0.032	0.021	0.014	0.008	0.004
B8								1	0.030	0.019	0.013	0.008	0.004
B9									1	0.021	0.014	0.008	0.004
B10										1	0.014	0.009	0.005
B11											1	0.008	0.004
B12												1	0.003
B13													1

Table 25: The correlation matrix for the point-to-point uncertainties (systematic only) for the forward-central dijet measurements (Topology B). The relative luminosity and beam polarization uncertainties are not included because they are the same for all points.

Label	C1	C2	C3	C4	C5	C6	C7	C8	C9	C10	C11	C12	C13*
B1	0.009	0.020	0.024	0.027	0.025	0.020	0.018	0.014	0.010	0.006	0.004	0.003	-
B2	0.000	0.086	0.105	0.115	0.107	0.086	0.078	0.059	0.043	0.028	0.018	0.011	-
B3	0.000	0.000	0.044	0.048	0.045	0.036	0.032	0.024	0.018	0.011	0.008	0.004	-
B4	0.000	0.000	0.000	0.077	0.072	0.058	0.052	0.039	0.029	0.018	0.012	0.007	-
B5	0.000	0.000	0.000	0.000	0.066	0.053	0.048	0.036	0.026	0.017	0.011	0.007	-
B6	0.000	0.000	0.000	0.000	0.000	0.044	0.040	0.030	0.022	0.014	0.009	0.005	-
B7	0.000	0.000	0.000	0.000	0.000	0.000	0.038	0.029	0.021	0.014	0.009	0.005	-
B8	0.000	0.000	0.000	0.000	0.000	0.000	0.000	0.027	0.020	0.013	0.008	0.005	-
B9	0.000	0.000	0.000	0.000	0.000	0.000	0.000	0.000	0.022	0.015	0.010	0.006	-
B10	0.000	0.000	0.000	0.000	0.000	0.000	0.000	0.000	0.000	0.017	0.011	0.007	-
B11	0.000	0.000	0.000	0.000	0.000	0.000	0.000	0.000	0.000	0.000	0.010	0.006	-
B12	0.000	0.000	0.000	0.000	0.000	0.000	0.000	0.000	0.000	0.000	0.000	0.005	-
B13	0.000	0.000	0.000	0.000	0.000	0.000	0.000	0.000	0.000	0.000	0.000	0.000	-

Table 26: The correlation matrix for the point-to-point uncertainties (systematic only) coupling forward-central dijet measurements (Topology B) with central-central dijet measurements (Topology C). The relative luminosity and beam polarization uncertainties are not included because they are the same for all points.

Label	D1*	D2	D3	D4	D5	D6	D7	D8	D9	D10	D11	D12	D13
B1	-	0.031	0.043	0.050	0.050	0.041	0.038	0.030	0.022	0.015	0.010	0.006	0.003
B2	-	0.055	0.076	0.088	0.087	0.072	0.066	0.052	0.039	0.026	0.017	0.010	0.006
B3	-	0.000	0.048	0.055	0.055	0.046	0.042	0.033	0.025	0.016	0.011	0.007	0.004
B4	-	0.000	0.000	0.134	0.133	0.111	0.102	0.079	0.060	0.039	0.027	0.016	0.009
B5	-	0.000	0.000	0.000	0.118	0.098	0.090	0.070	0.053	0.035	0.024	0.014	0.008
B6	-	0.000	0.000	0.000	0.000	0.075	0.069	0.054	0.040	0.027	0.018	0.011	0.006
B7	-	0.000	0.000	0.000	0.000	0.000	0.062	0.048	0.036	0.024	0.016	0.010	0.005
B8	-	0.000	0.000	0.000	0.000	0.000	0.000	0.041	0.031	0.021	0.014	0.008	0.005
B9	-	0.000	0.000	0.000	0.000	0.000	0.000	0.000	0.029	0.019	0.013	0.008	0.004
B10	-	0.000	0.000	0.000	0.000	0.000	0.000	0.000	0.000	0.018	0.012	0.007	0.004
B11	-	0.000	0.000	0.000	0.000	0.000	0.000	0.000	0.000	0.000	0.011	0.007	0.004
B12	-	0.000	0.000	0.000	0.000	0.000	0.000	0.000	0.000	0.000	0.000	0.005	0.003
B13	-	0.000	0.000	0.000	0.000	0.000	0.000	0.000	0.000	0.000	0.000	0.000	0.007

Table 27: The correlation matrix for the point-to-point uncertainties (systematic only) coupling forward-central dijet measurements (Topology B) with forward-backward dijet measurements (Topology D). The relative luminosity and beam polarization uncertainties are not included because they are the same for all points.

Label	C1	C2	C3	C4	C5	C6	C7	C8	C9	C10	C11	C12	C13*
C1	1	0.020	0.025	0.026	0.024	0.019	0.017	0.013	0.009	0.006	0.004	0.002	-
C2		1	0.183	0.196	0.181	0.145	0.130	0.097	0.070	0.045	0.030	0.018	-
C3			1	0.028	0.026	0.021	0.019	0.014	0.010	0.006	0.004	0.003	-
C4				1	0.058	0.046	0.041	0.031	0.022	0.014	0.009	0.006	-
C5					1	0.038	0.034	0.025	0.018	0.012	0.008	0.005	-
C6						1	0.027	0.020	0.014	0.009	0.006	0.004	-
C7							1	0.019	0.014	0.009	0.006	0.004	-
C8								1	0.013	0.008	0.006	0.003	-
C9									1	0.010	0.007	0.004	-
C10										1	0.009	0.005	-
C11											1	0.005	-
C12												1	-
C13													-

Table 28: The correlation matrix for the point-to-point uncertainties (systematic only) for the central-central dijet measurements (Topology C). The relative luminosity and beam polarization uncertainties are not included because they are the same for all points.

Label	D1*	D2	D3	D4	D5	D6	D7	D8	D9	D10	D11	D12	D13
C1	-	0.032	0.044	0.050	0.049	0.040	0.037	0.028	0.021	0.014	0.009	0.006	0.003
C2	-	0.097	0.134	0.152	0.150	0.123	0.113	0.087	0.065	0.043	0.029	0.017	0.010
C3	-	0.000	0.029	0.033	0.032	0.027	0.024	0.019	0.014	0.009	0.006	0.004	0.002
C4	-	0.000	0.000	0.110	0.108	0.089	0.082	0.063	0.047	0.031	0.021	0.012	0.007
C5	-	0.000	0.000	0.000	0.087	0.071	0.065	0.050	0.037	0.025	0.017	0.010	0.006
C6	-	0.000	0.000	0.000	0.000	0.051	0.047	0.036	0.027	0.018	0.012	0.007	0.004
C7	-	0.000	0.000	0.000	0.000	0.000	0.042	0.032	0.024	0.016	0.011	0.006	0.004
C8	-	0.000	0.000	0.000	0.000	0.000	0.000	0.028	0.021	0.014	0.009	0.006	0.003
C9	-	0.000	0.000	0.000	0.000	0.000	0.000	0.000	0.020	0.013	0.009	0.005	0.003
C10	-	0.000	0.000	0.000	0.000	0.000	0.000	0.000	0.000	0.014	0.010	0.006	0.003
C11	-	0.000	0.000	0.000	0.000	0.000	0.000	0.000	0.000	0.000	0.008	0.005	0.003
C12	-	0.000	0.000	0.000	0.000	0.000	0.000	0.000	0.000	0.000	0.000	0.005	0.003
C13*	-	-	-	-	-	-	-	-	-	-	-	-	-

Table 29: The correlation matrix for the point-to-point uncertainties (systematic only) coupling central-central dijet measurements (Topology C) with forward-backward dijet measurements (Topology D). The relative luminosity and beam polarization uncertainties are not included because they are the same for all points.

Label	D1*	D2	D3	D4	D5	D6	D7	D8	D9	D10	D11	D12	D13
D1*	-												
D2		1	0.097	0.115	0.120	0.103	0.096	0.077	0.059	0.040	0.027	0.017	0.009
D3			1	0.038	0.040	0.034	0.032	0.025	0.019	0.013	0.009	0.005	0.003
D4				1	0.197	0.168	0.158	0.125	0.097	0.065	0.045	0.027	0.015
D5					1	0.130	0.122	0.097	0.075	0.050	0.034	0.021	0.012
D6						1	0.082	0.065	0.050	0.034	0.023	0.014	0.008
D7							1	0.054	0.042	0.028	0.019	0.012	0.007
D8								1	0.032	0.022	0.015	0.009	0.005
D9									1	0.018	0.012	0.007	0.004
D10										1	0.011	0.007	0.004
D11											1	0.006	0.003
D12												1	0.003
D13													1

Table 30: The correlation matrix for the point-to-point uncertainties (systematic only) for the forward-backward dijet measurements (Topology D). The relative luminosity and beam polarization uncertainties are not included because they are the same for all points.